IEEE Access
Multidisciplinary | Rapid Review | Open Access Journal

Received July 15, 2019, accepted July 24, 2019, date of publication August 1, 2019, date of current version August 14, 2019.

Digital Object Identifier 10.1109/ACCESS.2019.2932612

Sparse With Fast MM Superresolution Algorithm for Radar Forward-Looking Imaging

QIPING ZHANG, (Student Member, IEEE), YIN ZHANG, (Member, IEEE), YULIN HUANG, (Senior Member, IEEE), YONGCHAO ZHANG, (Member, IEEE), WENCHAO LI, (Member, IEEE), AND JIANYU YANG, (Member, IEEE)

School of Information and Communication Engineering, University of Electronic Science and Technology of China, Chengdu 611731, China

Corresponding author: Yin Zhang (yinzhang@uestc.edu.cn)

This work was supported by the National Natural Science Foundation of China under Grant 61671117.

ABSTRACT The problem of low azimuth resolution has restricted the applicability for radar forward-looking imaging in practice. In this paper, a sparse with fast majorization-minimization (SFMM) superresolution algorithm was proposed to realize fast superresolution imaging of sparse targets in radar forward-looking area. First, we analyzed the azimuth signal of the radar forward-looking area and modeled the azimuth signal as a convolution of antenna pattern and targets distribution. Second, the superresolution problem was converted into an L_1 regularization issue by introducing the L_1 norm to represent the distribution of the targets under the regularization framework. Third, according to the principle of majorization-minimization (MM) algorithm, a simple L_2 regularization issue was obtained to replace the difficult L_1 one, and the real target distribution was obtained by solving the L_2 regularization problem (We named it sparse with MM (SMM) superresolution algorithm for convenience). Then, in order to improve the computational efficiency of the algorithm, we adopted the second-order vector extrapolation idea to accelerate the conventional MM algorithm and solve the L_2 regularization problem. The simulation and real data verified that the proposed SFMM algorithm not only improves the azimuth resolution in radar forward-looking imaging but also increases convergence speed on the basis of SMM superresolution algorithm.

INDEX TERMS Superresolution, radar imaging, majorization-minimization, vector extrapolation.

I. INTRODUCTION

Radar has been widely used in many military and civilian fields for its all-day and all-weather imaging ability [1], [2]. In precision guidance, autonomous landing and topographic mapping, etc., we expect to obtain the accurate information of interested targets in forward-looking area, so the forward-looking region superresolution imaging is extremely important [3], [4]. However, the traditional technologies, such as synthetic aperture radar (SAR) and Doppler beam sharpening (DBS), can not realize forward-looking imaging due to the Doppler ambiguity [5], [6]. The bistatic SAR whose transmitter and receiver are mounted on separate platforms can be used to realize forward-looking imaging [7]–[9], but it is confronted with complicated processing problems, such as synchronization and motion compensation.

The associate editor coordinating the review of this manuscript and approving it for publication was Xian Sun.

The real aperture radar can achieve forward-looking imaging by antenna scanning in imaging region, but its azimuth resolution is limited to antenna size in practice [10], [11]. Currently, it has been confirmed that the azimuth signal of real aperture radar forward-looking imaging can be modeled as a convolution of targets distribution and antenna pattern, so the azimuth resolution can be improved by deconvolution methods [12], [13]. However, the deconvolution is ill-posed, its inverse thus being highly noise sensitive. In previous research, many methods haven been proposed to relax the ill-posedness of deconvolution and have achieved some results, such as Wiener filtering [14], Richardson-Lucy [15], truncated singular value decomposition (TSVD) [16], etc, but the resolution improvement of these methods are limited. The spectrum-estimation-based methods, such as the multiple signal classification (MUSIC) algorithm and minimum-variance beamforming technique, have been introduced in [17], [18], but these algorithms need lots of snapshots and are usually used for estimating the direction of arrival of point target.

The iterative adaptive approach (IAA) is an iterative weighted least squares approach for angular superresolution, which remarkably improves the azimuth angular resolution with just one snapshot, but it faces the problem of high computational complexity [13], [19].

Recently, the sparse regularization is a widely used method to relax ill-posedness and achieve superresolution [20], [21]. It improves the resolution by introducing targets prior information under regularization framework [22], [23]. In radar forward-looking imaging, usually the targets of interest are sparse compared with whole imaging region. Therefore, the sparse regularization method is suitable to improve the azimuth resolution for radar forward-looking imaging. The core of sparse regularization method is to select a reasonable prior information of sparse targets. For this purpose, most research chose a convex L_1 norm to represent the targets sparsity under regularization framework [24], [25], then a L_1 regularization problem was obtained, and the superresolution was achieved by solving it using convex optimization method. Because the L_1 norm is not differentiable, solving L_1 regularization issue is a challenging task. Although some alternative technologies, such as iterative shrinkage threshold (IST) algorithm [26], split Bregman (SB) algorithm [27], augmented Lagrange method [28], etc, have been proposed, they inevitably minimize the L_1 regularization issue. The majorization-minimization (MM) algorithm, which substitutes a simple optimization problem for a difficult optimization problem and turns a nondifferentiable problem into a smooth one [29], [30], is easier to obtain the solution of difficult optimization problem than above methods. For the difficult L_1 regularization problem, one would see that the MM algorithm can linearize it into an easy L_2 regularization issue in flowing section, so it is easy to be minimized. However, traditional MM algorithm needs large iterations because of its low convergence speed, so the processing efficiency is limited in radar real-time imaging. Accordingly, the research of how to improve the efficiency of the MM algorithm is of great value in practice.

At present, to accelerate an algorithm, one strategy is based on the matrix analysis. This strategy reduces the time of each iteration by fast solving the linear equations according to the special structure of coefficient matrix, such as Toplitz structure [31], Hankel structure [32], etc. Another strategy is to reduce the iterations based on vector extrapolation. This strategy employs previous and current iterative results to extrapolate a big direction vector and predict an optimal iteration point for next iteration, which benefits to convergence to the optimal solution faster [33], [34]. In our research, the convergence rate of the conventional MM algorithm is unsatisfactory, so the second strategy would realize better performance improvement in processing efficiency. In this paper, a sparse with fast majorization-minimization (SFMM) superresolution algorithm was proposed to improve the azimuth resolution of sparse targets in radar forward-looking imaging. The proposed method essentially is an improvement of traditional L_1 regularization method. In this work, the difficult L_1 regularization problem was simplified to a smooth L_2 regularization problem according to the MM principle. Then we used the second-order vector extrapolation to improve the convergence speed of traditional MM algorithm, which greatly improved the computational efficiency. Finally, we conducted some simulations and real data processing to verify the superior performance of the proposed SFMM algorithm.

The structure of this paper was as follows. In section II, we analyzed the signal model of real aperture radar forward-looking imaging. One can see that its azimuth signal can be built as a convolution of targets distribution and antenna pattern. In section III, the proposed SFMM algorithm would be deduced. In this section, we first built the convex optimization model by introducing the L_1 norm under regularization framework. Then the traditional MM algorithm was employed to solve the convex optimization problem. After that, we used a second-order expansion strategy to accelerate the traditional MM algorithm and obtained the proposed SFMM algorithm. Finally, the selection of the regularization parameter was discussed. Section IV verified the performance of the proposed SFMM algorithm by experiments, which included simulations and real data. The conclusion was discussed in section V.

II. SIGNAL MODEL

To realize forward-looking imaging, the radar works in scanning model, and its antenna scans the imaging region all the time. For moving platform imaging, its geometric configuration is shown in FIGURE 1, where $[-\Phi, \Phi]$ is the imaging region, ω is the scanning speed, so we can obtain the sampling number in azimuth is $N = 2\Phi/\omega$, where N is the sampling number in azimuth. Besides, θ_0 and R_0 are the scanning angle and range distance, respectively, at the initial time, $\theta(t)$ and $R(t)$ are the scanning angle and range distance at time t.

From FIGURE 1, the range history of a target P is expressed as

$$R(t) = \sqrt{{R_0}^2 + V^2t^2 - 2R_0Vt\cos\theta_0} \tag{1}$$

Its Taylor expansion is

$$R(t) \approx R_0 - V\cos\theta_0 t + \frac{V^2\sin{\theta_0}^2}{2R_0}t^2 \tag{2}$$

In forward-looking imaging, the range distance is usually large, which makes the quadratic term in Eq. (2) much smaller than $R_0 - V\cos\theta_0 t$, so Eq. 2 can be simplified as [35]

$$R(t) \approx R_0 - V\cos\theta_0 t \tag{3}$$

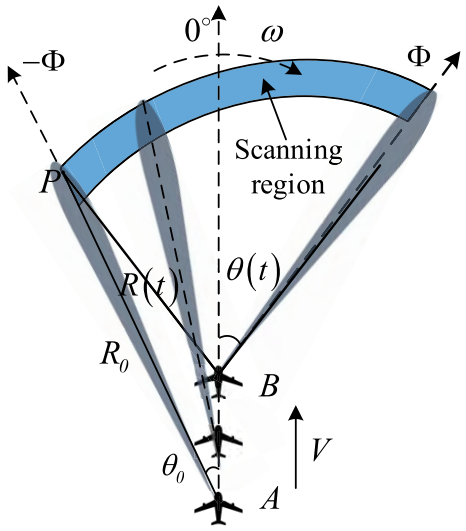

FIGURE 1. Geometric configuration of radar forward-looking imaging.

The radar transmits linearized frequency modulation (LFM) signal. Then after scanning, the received signal is

$$y(t,\tau) = \sum_{j=1}^{M}\sum_{i=1}^{N}\sigma_{ij}x(t)\,rect\left(\frac{\tau-\tau_d}{T}\right)\exp\left[j\pi K_p(\tau-\tau_d)^2\right] \times \exp\left(-j\pi\frac{4R(t)}{\lambda}\right) \tag{4}$$

where $y(\cdot)$ represents the received signal, t and τ represent the slow time and fast time, respectively, where the slow time denotes the time change in the angular dimension, which is related to the antenna scanning, and the fast time denotes the time change in the range dimension, which depends on the light speed, M and N are the sampling number in range and azimuth, respectively, $\sigma_{i,j}$ is the amplitude of the i,jth target, $x(t)$ is the modulation of antenna pattern, $rect(\cdot)$ is a rectangular window function, T the pulse width, K_p is the chirp rate, λ is the wave length, and τ_d is the time delay which can be expressed as τ_d=$2R(t)/c$.

After pulse compression and range walk correction, the received signal can be written as

$$y(R,\theta) = \sum_{i=1}^{M}\sum_{j=1}^{N}\sigma_{i,j}\widetilde{A}(\theta-\theta_0)\,sinc\left[\frac{2B}{c}(R-R_0)\right] \times \exp\left(-j\frac{4\pi}{\lambda}V\frac{\theta-\theta_0}{\omega}\right) \tag{5}$$

where $\theta = \theta_0 + \omega t$, $\exp\left(-j\frac{4\pi}{\lambda}V\frac{\theta-\theta_0}{\omega}\right)$ is the Doppler shift.

For static platform, we can see that the Doppler shift equals zero. For the motion platform with low speed moving or high speed scanning, the Doppler shift only has small effect to the received signal. As a result, it is usually negligible in practice. Then, the received signal (5) can be written as a convolution, i.e,

$$y(R,\theta) = h(R,\theta)\otimes\sigma(R,\theta) \tag{6}$$

with

$$h(R,\theta)\,\theta = \widetilde{A}(\theta)\,sinc\left(\frac{2B}{c}R\right) \tag{7}$$

For convenience, the convolution model expressed in Eq. (6) can be rewritten as a product of matrix and vector (Considering the noise), i.e,

$$\boldsymbol{y} = \boldsymbol{A}\boldsymbol{\sigma} + \boldsymbol{n} \tag{8}$$

where $\boldsymbol{y}$ is the received signal, $\boldsymbol{A}$ is the convolution matrix, $\boldsymbol{\sigma}$ is the targets distribution, and $\boldsymbol{n}$ is the noise.

III. Algorithm

In this section, we research the traditional SMM algorithm and use a second-order extrapolation strategy to accelerate it. The research is started by introducing the regularization model for sparse superresolution problem.

A. REGULARIZATION MODEL FOR SPARSE SUPERRESOLUTION PROBLEM

To estimate real targets $\boldsymbol{\sigma}$ from the noise-polluted real beam echo $\boldsymbol{y}$ is usually ill-posed, thus yielding highly noise-sensitive solutions. To relax the ill-posedness, a typical regularization criteria is written as

$$\widehat{\boldsymbol{\sigma}} = \min_{\boldsymbol{\sigma}}\frac{1}{2}\|\boldsymbol{A}\boldsymbol{\sigma}-\boldsymbol{y}\|_2^2 + \mu f(\boldsymbol{\sigma}) \tag{9}$$

where $\widehat{\boldsymbol{\sigma}}$ is the estimation of $\boldsymbol{\sigma}$, μ is the regularization parameter which controls the weight added to the regularizer, $f(\boldsymbol{\sigma})$ denotes a penalty function expressing the targets prior information, and the use of penalty function was expected to constraint the range of solutions thereby suppressing the noise amplification. Recent research have proposed many penalty functions according to different targets prior, such as L_p, total variation (TV), low rank (LK) [36], etc.

For sparse superresolution problem, usually the L_p norm with $0 \le p \le 1$ was employed as penalty function. We know that the stronger sparsity needs a smaller p. However, the situation $p = 0$ leads to a N-P hard problem and it is very difficult to solve. Besides, a non-convex problem would to be solved with $0 < p < 1$, and finding the globally optimal solution is also N-P hard. Therefore, in this work, we selected the convex L_1 norm to represent the sparsity of targets, then the regularization model is

$$\widehat{\boldsymbol{\sigma}} = \min_{\boldsymbol{\sigma}}\frac{1}{2}\|\boldsymbol{A}\boldsymbol{\sigma}-\boldsymbol{y}\|_2^2 + \mu\|\boldsymbol{\sigma}\|_1 \tag{10}$$

B. SOLUTION BY MM ALGORITHM

To solve the problem in (10), the MM algorithm requires to replace it by a finite-dimensional optimization problem, i.e,

$$\widehat{\boldsymbol{\sigma}} = \min_{\boldsymbol{\sigma}} L(\boldsymbol{\sigma}) \tag{11}$$

where

$$L(\boldsymbol{\sigma}) = \frac{1}{2}\|\boldsymbol{A}\boldsymbol{\sigma}-\boldsymbol{y}\|_2^2 + \mu\|\boldsymbol{\sigma}\|_1 \tag{12}$$

The function $L(\boldsymbol{\sigma})$ is called cost function, and we note that it's convex but nondifferentiable.

Because the cost function $L(\boldsymbol{\sigma})$ is not differentiable, it is not easy to obtain its solution. Using the MM idea, we would minimize a succedaneous function $G\left(\boldsymbol{\sigma}|\boldsymbol{\sigma}^k\right)$ that easier to be solved. So the key of the MM algorithm is to specify the function $G\left(\boldsymbol{\sigma}|\boldsymbol{\sigma}^k\right)$ which is easier to be minimized and also approximate $L(\boldsymbol{\sigma})$, i.e

$$\boldsymbol{\sigma}^{k+1} = \min_{\boldsymbol{\sigma}} G\left(\boldsymbol{\sigma}|\boldsymbol{\sigma}^k\right) \tag{13}$$

where

$$G\left(\boldsymbol{\sigma}|\boldsymbol{\sigma}^k\right) \geq L(\boldsymbol{\sigma}) \tag{14}$$

for all $\boldsymbol{\sigma}$, and

$$G(\boldsymbol{\sigma}|\boldsymbol{\sigma}) = L(\boldsymbol{\sigma}) \tag{15}$$

From Eq. (14) and (15), the function $G\left(\boldsymbol{\sigma}|\boldsymbol{\sigma}^k\right)$ is an upper band for $L(\boldsymbol{\sigma})$, and it ensures that the iterative value $L\left(\boldsymbol{\sigma}^k\right)$ is monotonically decreasing, which makes the MM algorithm converge to optimization, i.e,

$$\begin{aligned} L\left(\boldsymbol{\sigma}^{k+1}\right) &= L\left(\boldsymbol{\sigma}^{k+1}\right) - G\left(\boldsymbol{\sigma}^{k+1}|\boldsymbol{\sigma}^k\right) + G\left(\boldsymbol{\sigma}^{k+1}|\boldsymbol{\sigma}^k\right) \\ &\leq G\left(\boldsymbol{\sigma}^{k+1}|\boldsymbol{\sigma}^k\right) \\ &\leq G\left(\boldsymbol{\sigma}^{k}|\boldsymbol{\sigma}^k\right) \\ &= L\left(\boldsymbol{\sigma}^{k}\right) \end{aligned} \tag{16}$$

For the MM algorithm to succeed, the core is to choose an appropriate upper band of the cost function. In this work, we want to select a function $G\left(\boldsymbol{\sigma}|\boldsymbol{\sigma}^k\right)$ that satisfies (13), (14) and (15).

In (12), we can see that the difficulty of solving the problem comes from the L_1 norm $\|\boldsymbol{\sigma}\|_1$, so the upper band of $\|\boldsymbol{\sigma}\|_1$ needs to be specified firstly. For a function $f(t) = |t|$, an upper band can be chosen as a quadratic function, i.e: $g(t) = at^2 + b$, which satisfies $g(t) \geq f(t)$ for all t and $g\left(t^k\right) = f\left(t^k\right)$, as Fig. 2 shows. Especially, at $t = t^k$, the upper band can be chosen as [37]:

$$g(t) = \frac{1}{2\left|t^k\right|}t^2 + \frac{1}{2}\left|t^k\right| \tag{17}$$

Let $\sigma(n)$ for t and add all $\sigma(n)$, we have

$$\sum_n \left[\frac{1}{2\left|\sigma^k(n)\right|}\sigma^2(n) + \frac{1}{2}\left|\sigma^k(n)\right|\right] \geq \sum_n |\sigma(n)| \tag{18}$$

that is,

$$\frac{1}{2}\boldsymbol{\sigma}^T\boldsymbol{\Lambda}_k\boldsymbol{\sigma} + \frac{1}{2}\left\|\boldsymbol{\sigma}^k\right\|_1 \geq \|\boldsymbol{\sigma}\|_1 \tag{19}$$

where $\boldsymbol{\Lambda}_k = diag\left(1/\left|\boldsymbol{\sigma}^k\right|\right)$.

Accordingly, using the MM idea, the objective function in Eq. (13) can be specified as

$$G\left(\boldsymbol{\sigma}|\boldsymbol{\sigma}^k\right) = \frac{1}{2}\|\boldsymbol{A}\boldsymbol{\sigma} - \boldsymbol{y}\|_2^2 + \frac{\mu}{2}\boldsymbol{\sigma}^T\boldsymbol{\Lambda}_k^{-1}\boldsymbol{\sigma} + \frac{\mu}{2}\left\|\boldsymbol{\sigma}^k\right\|_1 \tag{20}$$

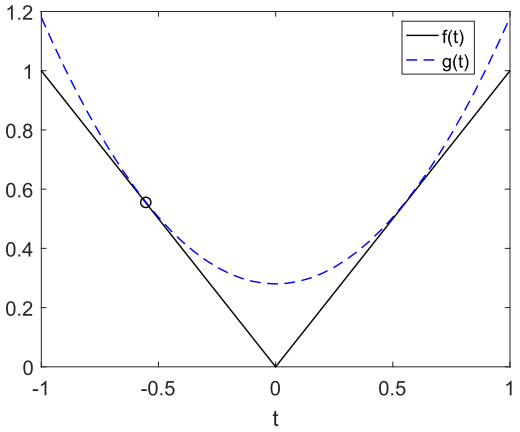

FIGURE 2. Upper band of $f(x)$.

Removing the constant term, the MM algorithm update (13) for $\boldsymbol{\sigma}^k$ is

$$\boldsymbol{\sigma}^{k+1} = \min_{\boldsymbol{\sigma}} \frac{1}{2}\|\boldsymbol{A}\boldsymbol{\sigma} - \boldsymbol{y}\|_2^2 + \frac{\mu}{2}\boldsymbol{\Lambda}_k\|\boldsymbol{\sigma}\|_2^2 \tag{21}$$

where

$$\boldsymbol{\Lambda}_k = diag\left(\frac{\mu}{\left|\boldsymbol{\sigma}^k\right|}\right) \tag{22}$$

Obviously, using the MM algorithm, the difficult L_1 regularization problem (11) and (12) have been converted into an easy L_2 regularization problem (21). It can be easily solved by iterating

$$\boldsymbol{\sigma}^{k+1} = \left(\boldsymbol{A}^T\boldsymbol{A} + \boldsymbol{\Lambda}_k\right)^{-1}\boldsymbol{A}^T\boldsymbol{y} \tag{23}$$

C. SOLUTION BY FMM ALGORITHM

Although the problem (21) can be directly minimized by (23), this iterative technique operates on the result of the previous iteration and are normally slow to converge toward the final result, resulting in large iterations. In this section, a fast MM (FMM) algorithm based on vector extrapolation was used to accelerate the conventional MM algorithm.

The ideal of vector extrapolation is to predict the next iteration using the current and previous iterative information to extrapolate a big vector, thus converging to the optimization solutions faster. This process was shown in FIGURE 3.

In FIGURE 3, $\boldsymbol{\sigma}^k$ is iterated point, $\boldsymbol{v}^k$ the predicted point, $\boldsymbol{d}^k$ is the direction vector defined as

$$\boldsymbol{d}^k = \boldsymbol{\sigma}^k - \boldsymbol{\sigma}^{k-1} \tag{24}$$

For a minimization problem $\widehat{\boldsymbol{\sigma}} = \min_{\boldsymbol{\sigma}} f(\boldsymbol{\sigma})$, we supposed that its optimization solution can be obtained by iterating $\boldsymbol{\sigma}^{k+1} = \xi\left(\boldsymbol{\sigma}^k\right)$. According to vector extrapolation idea, the predicted point in current iteration can be obtained by Taylor expansion,

$$\boldsymbol{v}^k = \boldsymbol{\sigma}^k + \alpha_k\nabla\boldsymbol{\sigma}^k + \frac{1}{2!}\alpha_k^2\nabla^2\boldsymbol{\sigma}^k + \cdots + \frac{1}{n!}\alpha_k^n\nabla^n\boldsymbol{\sigma}^k \tag{25}$$

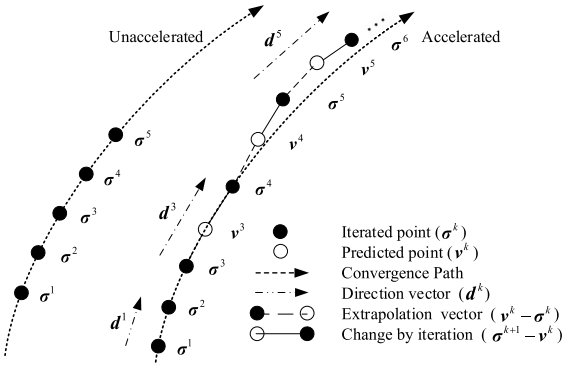

FIGURE 3. Vector extrapolation diagram.

where α_k is acceleration parameter, $\nabla^n\boldsymbol{\sigma}^k$ is the n-order difference at point $\boldsymbol{\sigma}^k$. After that, the accelerated algorithm can be realized by iterating

$$\boldsymbol{\sigma}^{k+1}=\xi\left(\boldsymbol{v}^k\right) \tag{26}$$

In fact, higher-order Taylor expansion of $\boldsymbol{v}^k$ provides more accurate predicted point or faster acceleration for above acceleration algorithm. However, it results in high computational complexity to obtain an accurate acceleration parameter α_k. So in recent research, only the first and second Taylor expansions were used [33].

Another key problem of this acceleration algorithm is to select a reasonable acceleration parameter. The acceleration parameter provides correction step to adjust the step length and further guarantee the stability of the solutions. To use the two-order acceleration, it has been proved that the acceleration parameter was expressed as [33]

$$\alpha^k=\sqrt{\frac{\left(\boldsymbol{d}^{k-1}\right)^T\boldsymbol{d}^{k-1}}{\left(\boldsymbol{d}^{k-2}\right)^T\boldsymbol{d}^{k-2}}},\quad 0<\alpha^k<1 \tag{27}$$

In our work, the two-order vector extrapolation was used to accelerate the traditional MM algorithms. We let $\boldsymbol{\sigma}^k$ be the iterated point, $\boldsymbol{v}^k$ the predicted point, then the second order Taylor expansion of $\boldsymbol{v}^k$ at point $\boldsymbol{\sigma}^k$ is

$$\boldsymbol{v}^k=\boldsymbol{\sigma}^k+\alpha_k\nabla\boldsymbol{\sigma}^k+\frac{1}{2!}\alpha_k^2\nabla^2\boldsymbol{\sigma}^k \tag{28}$$

where $\nabla\boldsymbol{\sigma}^k$ is the gradient of $\boldsymbol{\sigma}^k$, $\nabla^2\boldsymbol{\sigma}^k$ is the second order gradient of $\boldsymbol{\sigma}^k$, which was defined as

$$\begin{aligned}\nabla^2\boldsymbol{\sigma}^k&=\nabla\boldsymbol{\sigma}^k-\nabla\boldsymbol{\sigma}^{k-1}\\&\quad+\left(\boldsymbol{\sigma}^k-\boldsymbol{\sigma}^{k-1}\right)-\left(\boldsymbol{\sigma}^{k-1}-\boldsymbol{\sigma}^{k-2}\right)\\&=\boldsymbol{\sigma}^k-2\boldsymbol{\sigma}^{k-1}+\boldsymbol{\sigma}^{k-2}\end{aligned} \tag{29}$$

Consequently, using the second-order vector extrapolation strategy, the proposed SFMM algorithm was listed in TABLE 1, where K is the iterations.

Compared with traditional SMM algorithm, the accelerated SFMM algorithm does not make the next iteration on the current iterated point $\boldsymbol{\sigma}^k$, but rather at the point $\boldsymbol{v}^k$ which relies on current point $\boldsymbol{\sigma}^k$ and previous point $\boldsymbol{\sigma}^{k-1}$. It can be found that the main computational complexity in the traditional SMM algorithm and accelerated SMM algorithm remains the same, namely in (23). For the accelerated SFMM algorithm, only two additional steps are requested to compute α^k and $\boldsymbol{v}^k$, which is marginal compared with the main computational complexity. However, the iterations of the traditional SMM algorithm were greatly reduced after acceleration, which would be verified in the next section.

TABLE 1. Flow chart of the proposed SFFM algorithm.

Initialize: $k=0,\ \boldsymbol{\sigma}^k=\boldsymbol{y}$

for k=1:2

$$\begin{aligned}\boldsymbol{\Lambda}_k&=diag\left(\mu/\left|\boldsymbol{\sigma}^k\right|\right)\\\boldsymbol{\sigma}^{k+1}&=\left(\boldsymbol{A}^T\boldsymbol{A}+\boldsymbol{\Lambda}_k\right)^{-1}\boldsymbol{A}^T\boldsymbol{y}\\\boldsymbol{d}^k&=\boldsymbol{\sigma}^k-\boldsymbol{\sigma}^{k-1}\end{aligned}$$

end

for k=3:K

$$\begin{aligned}\alpha^k&=\sqrt{\frac{\left(\boldsymbol{d}^{k-1}\right)^T\boldsymbol{d}^{k-1}}{\left(\boldsymbol{d}^{k-2}\right)^T\boldsymbol{d}^{k-2}}}\\\boldsymbol{v}^k&=\boldsymbol{\sigma}^k+\alpha_k\nabla\boldsymbol{\sigma}^k+\frac{1}{2!}\alpha_k^2\nabla^2\boldsymbol{\sigma}^k\\\boldsymbol{\Lambda}_k&=diag\left(\mu/\left|\boldsymbol{\sigma}^k\right|\right)\\\boldsymbol{\sigma}^{k+1}&=\left(\boldsymbol{A}^T\boldsymbol{A}+\boldsymbol{\Lambda}_k\right)^{-1}\boldsymbol{A}^T\boldsymbol{v}^k\\\boldsymbol{d}^k&=\boldsymbol{\sigma}^k-\boldsymbol{\sigma}^{k-1}\end{aligned}$$

end

D. SELECTION OF REGULARIZATION PARAMETER

For the proposed SFMM algorithm, we can see that its performance relies on the regularization parameter μ. We know that a small μ may lead to higher resolution, but the noise might be amplified. A large μ can smooth the noise, but leads to limited resolution improvement. So in practice, we need to select a reasonable regularization parameter to balance noise amplification and smoothness. In our work, the L-curve method was employed to select the regularization parameter μ [38], [39].

The L-curve method selects the regularization parameter by maximizing the curvature function:

$$J\left(\mu\right)=\frac{X''\left(\mu\right)Y'\left(\mu\right)-X'\left(\mu\right)Y''\left(\mu\right)}{\left[X'(\mu)^2+Y'(\mu)^2\right]^{3/2}} \tag{30}$$

where $X\left(\mu\right)=\log\left(\left\|\boldsymbol{A}\widehat{\boldsymbol{\sigma}}_\mu-\boldsymbol{y}\right\|_2\right)$, $Y\left(\mu\right)=\log\left(\left\|\nabla\left|\widehat{\boldsymbol{\sigma}}_\mu\right|\right\|_2\right)$, $\nabla\left(\cdot\right)$ is the gradient operator, and $\left('\right)$ denoting the differentiation with respect to μ.

TABLE 2. The system parameters of point target simulation.

Parameter	Value	Units
Beamwidth	2.5	°
Carrier frequency	10	GHz
Band width	15	MHz
Antenna scanning velocity	50	$^\circ/s$
Antenna scanning area	- 5 ∼ 5	°
Pulse repetition frequency	2000	Hz

IV. EXPERIMENTS

In this section, some experiments were conducted to prove the superior performance of the proposed algorithm. To verify the recovering ability, the experimental results are compared with some traditional superresolution methods, including TSVD [16] and iterative adaptive approach (IAA) [13] methods.

A. POINT TARGET SIMULATIONS

The experiments started from a point target simulation. We first employed two adjacent targets located at $-0.5°$ and $0.5°$, respectively, with same amplitude. The antenna pattern was a $sinc^2$ function which is defined as $sinc\,(x) = \sin(\pi x)/(\pi x)$, and its main lobe width is 2.5°. The system parameters are illustrated in TABLE 2.

The simulation results are shown in FIGURE 4. Because the noise can not be avoided in applications, the real beam echo was polluted by white Gaussian noise, and we let the SNR = 20dB. From the real beam echo, the adjacent targets can not be distinguished because their interval is smaller than antenna beam width. After superreoslution processing, the TSVD can partly distinguish adjacent targets, but the resolution is poor, and the side lobes increase. The IAA algorithm has better performance in resolution improvement than TSVD, so the adjacent targets were distinguished. However, compared with the SMM and SFMM methods, its noise suppression ability is limited. The sparse algorithms not only distinguishes adjacent targets, but also better suppress noise.

In addition, to quantitatively evaluate the superresolution performance of different algorithms, some performance indexes were listed in TABLE 3, including peak signal-to-noise ratio (PSNR) and image entropy. In this work, the *PSNR* was employed to appraise the noise suppression ability of different algorithms, and the image entropy was employed to evaluate the blur level of image since the entropy increase with the increase of image blurring level [40], [41]. The PSNR is defined as

$$PSNR = 20\log_{10}\frac{s_{\max}}{n_{\max}} \tag{31}$$

where s_{max} and n_{max} denote the maximum amplitude of signal and noise, respectively. From TABLE 3, we can firstly see that the SMM and SFMM methods can better suppress the noise thus have higher *PSNR* than other methods. Besides,

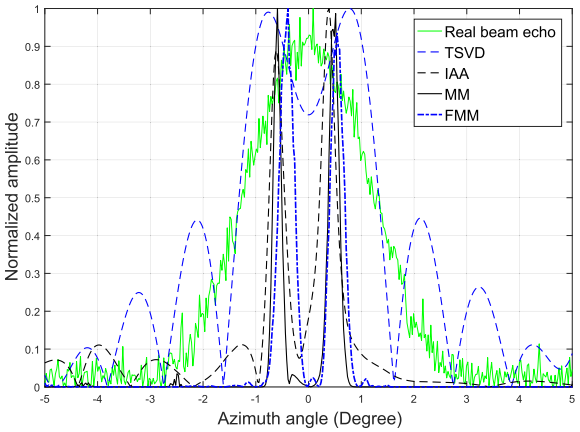

FIGURE 4. Point target simulation results.

TABLE 3. Performance indexes for FIGURE 4.

Method	PSNR (dB)	Image entropy	RT (s)
TSVD	7.1	4.6	0.043
IAA	19.16	4.29	0.259
SMM	29.14	1.43	0.619
SFMM	32.46	1.67	0.072

from the perspective of image entropy, we noted that the image entropy of the real beam echo is 6.7. After superresolution processing, the entropy of the results processed by SMM and SFMM algorithms are lower than those processed by TSVD and IAA, which indicates that the sparse methods can obtain clearer superresolution image than other methods. Although the image entropy of the result processed by the proposed SFMM algorithm is slightly higher than the result of SMM algorithm, their difference is small compared with the results of TSVD and IAA. Besides, the RT of the proposed SFMM algorithm seriously decrease compared with the SMM algorithm. Although the TSVD has faster processing speed than the proposed SFMM algorithm, its superresolution performance was much lower than the proposed SFMM algorithm.

B. AREA TARGET SIMULATION

In this section, an area target simulation was conducted to prove the performance of the proposed method. The original scene was shown in FIGURE 5(a), which is a fleet covering 11 boats. Compared with the whole imaging scene, these boats are sparse. The system parameters are listed in TABLE 4.

The simulation results are illustrated in FIGURE 5, where FIGURE 5(b) is the real beam echo whose SNR is 20dB. We can see that the real beam echo has low resolution, making the adjacent targets hard to be distinguished, and we can not distinguish how many targets are covered. After superresolution processing, the resolution was improved by TSVD, IAA and sparse methods. However, the resolution improvement

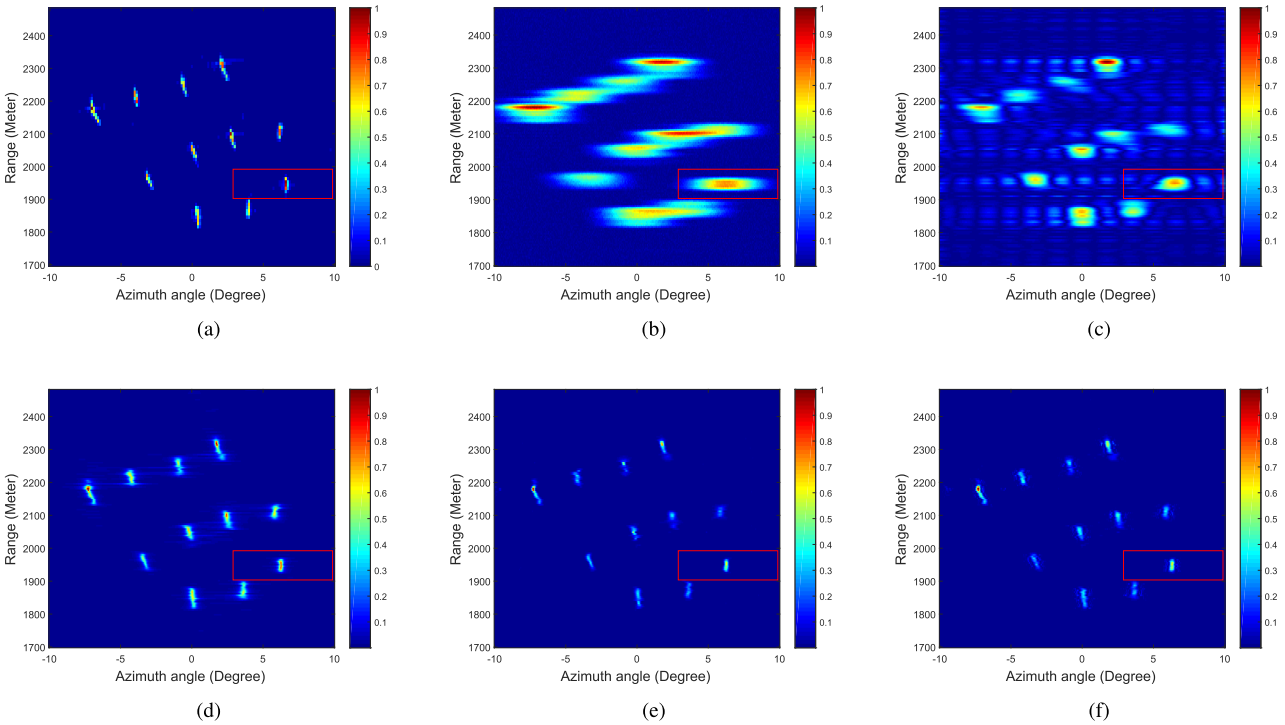

FIGURE 5. Results of area target simulation. (a) Original scene. (b) Real beam echo. (c) TSVD. (d) IAA. (e) SMM. (f) SFMM.

TABLE 4. The system parameters of area target simulation.

Parameter	Value	Units
Beamwidth	4	$^\circ$
Carrier frequency	37.5	GHz
Band width	12	MHz
Antenna scanning velocity	100	$^\circ/s$
Antenna scanning area	- 10 $\sim$ 10	$^\circ$
Pulse repetition frequency	2000	Hz

of TSVD is limited, and many side lobes increase, as FIGURE 5(c) shows. The IAA algorithm can further enhance the resolution, but some noise is enlarged, as FIGURE 5(d) shows. From FIGURE 5(e) and FIGURE 5(f), the sparse methods not only has higher resolution improvement than TSVD and IAA methods, but also suppress the noise.

In order to verify the above conclusion more intuitively, the profiles of FIGURE 5 was plotted in FIGURE 6, and the target area has been marked by red rectangle in FIGURE 5. From these profiles, it can be found that the sparse algorithms has better superresolution performance than the TSVD and IAA methods. They have better beam sharpening ability and noise suppression ability than other methods.

Similarly, the image entropy and RT were used to quantitatively evaluate the superresolution performance of different

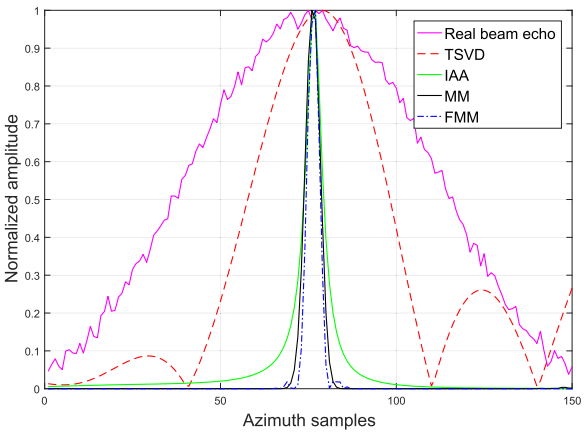

FIGURE 6. Profiles for FIGURE 5.

algorithms. From Fig. 6, we can see that the IAA also has good noise suppression ability, so the *PSNR* cannot reflect the performance of the proposed method. In area target simulation, the beam sharpening ration (BSR) was employed to evaluate the sharpening ability. In this paper, the BSR was defined as the ratio of main lobe sampling points between real beam echo and superresolution result. The performance indexes were shown in TABLE 5. From TABLE 5, we can see that the SMM and SFMM methods have better beam sharpening ability than other methods. As for image entropy and RT, we also noted that the image entropy of the real beam echo is 5.01, and the same conclusion was obtained as point target simulation.

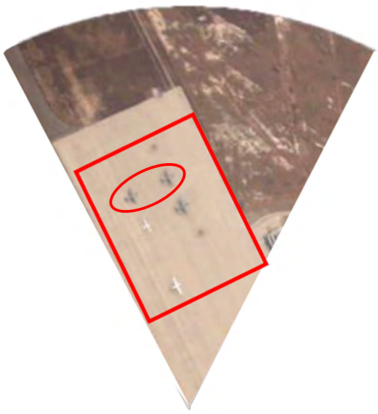

FIGURE 7. Original scene of real data.

FIGURE 8. Scene picture of the experiment.

TABLE 5. Performance indexes for FIGURE 5.

Method	BSR	Image entropy	RT (s)
TSVD	2	5.36	5.21
IAA	13.33	2.57	34.24
SMM	16	0.83	132.51
SFMM	16	0.92	13.11

C. REAL DATA PROCESSING

Above simulations have proved the superior performance of the proposed SFMM algorithm in sparse target imaging. In this section, a real data was further processed to verify its performance in practice.

The experiment was conducted in Pucheng, Xi'an, China. The original scene was an airport runway with 5 plants and 2 cars and have been marked by red rectangle, as FIGURE 7 shows. In this experiment, a X-band radar was hanged on a transport plane and was marked by red circle, as FIGURE 8 shows. The main system parameters of the radar were listed in TABLE 6.

FIGURE 9 illustrated the experimental results, where FIGURE. 9(a) is the real beam echo, and FIGURE 9(b) to 9(e)

TABLE 6. The system parameters of radar.

Parameter	Value	Units
Beamwidth	5.1	$^\circ$
Carrier frequency	9.4	GHz
Band width	75	MHz
Antenna scanning velocity	72	$^\circ/s$
Antenna scanning area	- 30 $\sim$ 30	$^\circ$
Pulse repetition frequency	200	Hz

TABLE 7. Performance indexes for FIGURE 9.

Method	PSNR (dB)	Image entropy	RT (s)
TSVD	7.74	3.63	6.07
IAA	18.42	0.42	57.87
SMM	32.76	0.24	191.27
SFMM	30.46	0.31	15.81

are the superresolution results processed by different algorithms. From the superresolution results, we can know that the real beam echo has low resolution and strong noise, making adjacent planes and cars almost undistinguishable. The TSVD method has poor resolution improvement, thus many false targets appear because of the elevation of side lobes. The IAA algorithm has better resolution enhancement than TSVD, but its performance is lower than SMM and SFMM algorithms. Besides, some false targets appeared in the result of IAA. Obviously, the noise level of IAA is higher than that of SMM and SFMM. As for the SMM and SFMM algorithms, they have greatly improved the resolution and suppressed the noise, so their results are clearer than others.

To prove above conclusions, the profiles of two adjacent targets marked by red circles in FIGURE 7 and 9 were illustrated in FIGURE 10. From the profiles, a high saddle and high side lobes remained in the profiles of real beam echo, TSVD and IAA results, resulting in low resolution. The SMM and SFMM algorithms can better distinguish the adjacent targets with low side lobes, but their performance was not the same.

According to the system parameters of the radar, we can know that the matrix size of the real beam echo is 1500×167. Similar to area target simulations, the relative performance indexes were showed in TABLE 7. Although TSVD has higher processing efficiency than IAA, SMM and SFMM algorithms, its *PSNR* was much lower than the IAA, SMM and SFMM algorithms. Even for the result of IAA, its *PSNR* was also much lower than the result of SMM and SFMM algorithms, demonstrating that the SMM and SFMM algorithms have better noise suppression ability than TSVD and IAA methods. As for the image entropy, we note that the image entropy of the real beam echo is 3.65. After supreresolution processing, the image entropy of SMM and SFMM algorithms are lower than TSVD and IAA. As for the SFMM algorithms, despite some performance degradation after

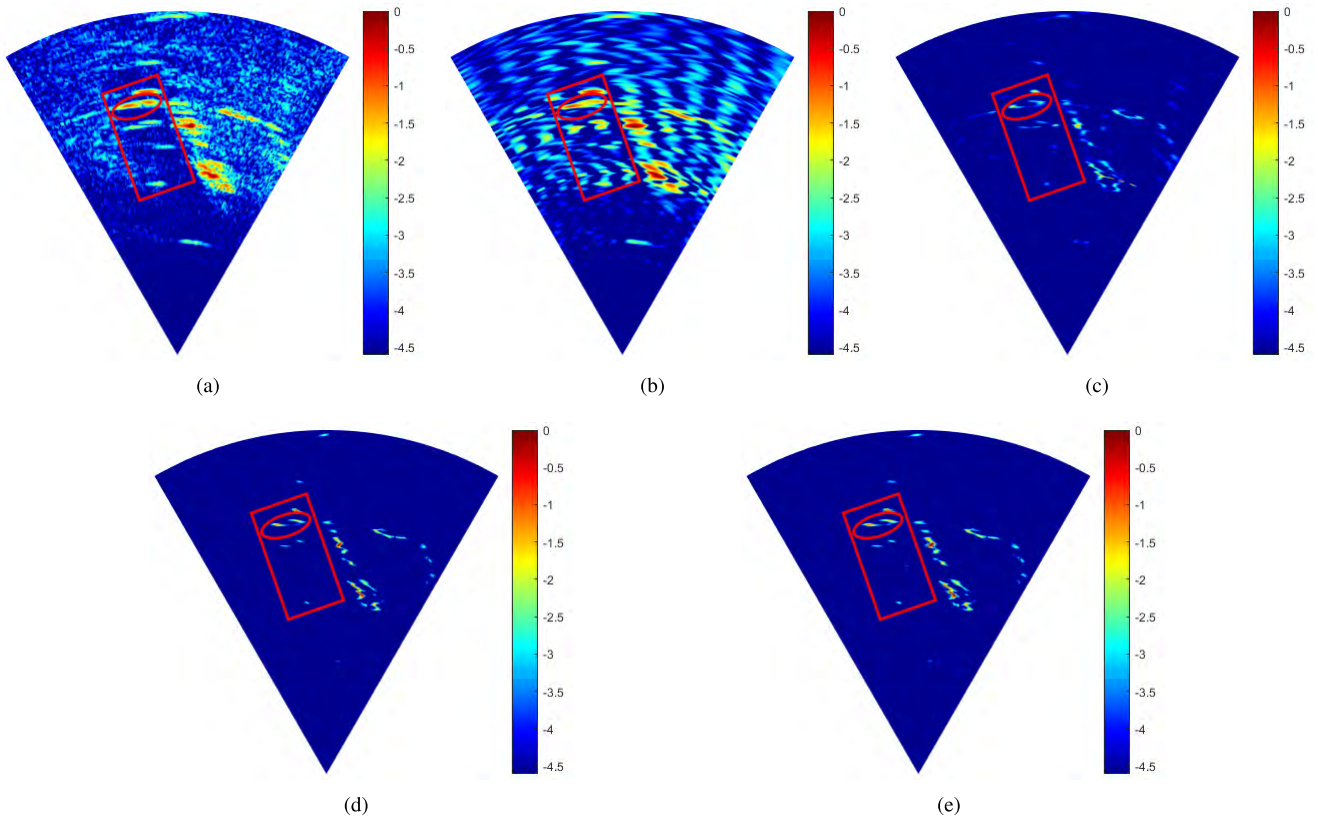

FIGURE 9. Results of area target simulation. (a) Real beam echo. (b) TSVD. (c) IAA. (d) SMM. (e) SFMM.

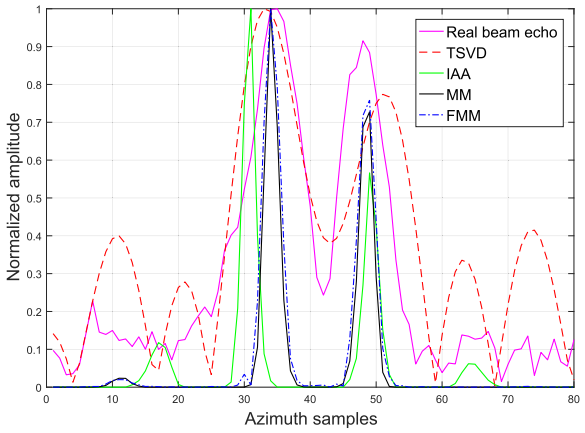

FIGURE 10. Two-targets' profiles for FIGURE 9.

accelerating, the RT was much less than SFMM algorithm, and the degradation was inappreciable compared with TSVD and IAA methods.

V. CONCLUSION

In this paper, we focused on the problem of low azimuth resolution in radar forward-looking imaging and proposed a SFMM algorithm to realize superresolution imaging. The proposed SFMM algorithm converts the difficult L_1 regularization problem to an easy L_2 problem according to MM idea. In addition, the acceleration based on second-order vector extrapolation reduced the iterations and RT of traditional SMM algorithm. From the simulations and real data, the proposed SFMM algorithm not only effectively enhanced the azimuth resolution and suppressed the noise, but also decreased the time cost compared with conventional SMM algorithm.

REFERENCES

[1] S. P. Jacobs and J. A. O'Sullivan, "Automatic target recognition using sequences of high resolution radar range-profiles," *IEEE Trans. Aerosp. Electron. Syst.*, vol. 36, no. 2, pp. 364–381, Apr. 2000.

[2] J. Wu, Z. Sun, H. An, J. Qu, and J. Yang, "Azimuth signal multichannel reconstruction and channel configuration design for geosynchronous spaceborne–airborne bistatic SAR," *IEEE Trans. Geosci. Remote Sens.*, vol. 57, no. 4, pp. 1861–1872, Apr. 2019.

[3] J. Balke, "Field test of bistatic forward-looking synthetic aperture radar," in *Proc. IEEE Int. Radar Conf.*, May 2005, pp. 424–429.

[4] M. R. Bradley, T. R. Witten, M. Duncan, and R. McCummins, "Mine detection with a forward-looking ground-penetrating synthetic aperture radar," *Proc. SPIE*, vol. 5089, pp. 334–348, Sep. 2003.

[5] J. Wu, Y. Li, W. Pu, Z. Li, and J. Yang, "An effective autofocus method for fast factorized back-projection," *IEEE Trans. Geosci. Remote Sens.*, vol. 57, no. 8, pp. 6145–6154, Aug. 2019.

[6] H. Chen, M. Li, P. Zhang, G. Liu, L. Jia, and Y. Wu, "Resolution enhancement for Doppler beam sharpening imaging," *IET Radar, Sonar Navigat.*, vol. 9, no. 7, pp. 843–851, Aug. 2015.

[7] J. Wu, J. Yang, Y. Huang, H. Yang, and H. Wang, "Bistatic forward-looking SAR: Theory and challenges," in *Proc. IEEE Radar Conf.*, May 2009, pp. 1–4.

[8] J. Wu, Z. Li, Y. Huang, J. Yang, H. Yang, and Q. H. Liu, "Focusing bistatic forward-looking SAR with stationary transmitter based on keystone transform and nonlinear chirp scaling," *IEEE Geosci. Remote Sens. Lett.*, vol. 11, no. 1, pp. 148–152, Jan. 2014.

[9] H. An, J. Wu, Z. Sun, and J. Yang, "A two-step nonlinear chirp scaling method for multichannel GEO spaceborne–airborne bistatic SAR spectrum reconstructing and focusing," *IEEE Trans. Geosci. Remote Sens.*, vol. 57, no. 6, pp. 3713–3728, Jun. 2019.
[10] J. Guan, Y. Huang, J. Yang, W. Li, and J. Wu, "Improving angular resolution based on maximum a posteriori criterion for scanning radar," in *Proc. IEEE Radar Conf.*, May 2012, pp. 0451–0454.
[11] S. Uttam and N. A. Goodman, "Superresolution of coherent sources in real-beam data," *IEEE Trans. Aerosp. Electron. Syst.*, vol. 46, no. 3, pp. 1557–1566, Jul. 2010.
[12] H. Dropkin and C. Ly, "Superresolution for scanning antenna," in *Proc. IEEE Nat. Radar Conf.*, May 1997, pp. 306–308.
[13] Y. Zhang, Y. Zhang, Y. Huang, J. Yang, and W. Li, "Super-resolution surface mapping for scanning radar: Inverse filtering based on the fast iterative adaptive approach," *IEEE Trans. Geosci. Remote Sens.*, vol. 56, no. 1, pp. 127–144, Jan. 2018.
[14] J. L. Álvarez-Pérez, S. J. Marshall, and K. Gregson, "Resolution improvement of ERS scatterometer data over land by Wiener filtering," *Remote Sens. Environ.*, vol. 71, no. 3, pp. 261–271, 2000.
[15] D. G. Dansereau, A. Eriksson, and J. Leitner, "Richardson-lucy deblurring for moving light field cameras," in *Proc. IEEE Conf. Comput. Vis. Pattern Recognit. Workshops*, Jul. 2017, pp. 70–81.
[16] Y. Wu, Y. Zhang, Y. Zhang, Y. Huang, and J. Yang, "TSVD with least squares optimization for scanning radar angular super-resolution," in *Proc. IEEE Radar Conf. (RadarConf)*, May 2017, pp. 1450–1454.
[17] K. Agarwal and R. Macháň, "Multiple signal classification algorithm for super-resolution fluorescence microscopy," *Nature Commun.*, vol. 7, Dec. 2016, Art. no. 13752.
[18] S. Markovich-Golan, A. Bertrand, M. Moonen, and S. Gannot, "Optimal distributed minimum-variance beamforming approaches for speech enhancement in wireless acoustic sensor networks," *Signal Process.*, vol. 107, pp. 4–20, Feb. 2015.
[19] Y. Zhang, Y. Zhang, Y. Huang, W. Li, and J. Yang, "Angular superresolution for scanning radar with improved regularized iterative adaptive approach," *IEEE Geosci. Remote Sens.*, vol. 13, no. 6, pp. 846–850, Jun. 2016.
[20] M. Simões, J. Bioucas-Dias, L. B. Almeida, and J. Chanussot, "A convex formulation for hyperspectral image superresolution via subspace-based regularization," *IEEE Trans. Geosci. Remote Sens.*, vol. 53, no. 6, pp. 3373–3388, Jun. 2015.
[21] W. Pu, J. Wu, X. Wang, Y. Huang, Y. Zha, and J. Yang, "Joint sparsity-based imaging and motion error estimation for BFSAR," *IEEE Trans. Geosci. Remote Sens.*, vol. 57, no. 3, pp. 1393–1408, Mar. 2019.
[22] J. Jiang, C. Chen, K. Huang, Z. Cai, and R. Hu, "Noise robust position-patch based face super-resolution via tikhonov regularized neighbor representation," *Inf. Sci.*, vols. 367–368, pp. 354–372, Nov. 2016.
[23] S. Tourbier, X. Bresson, P. Hagmann, J.-P. Thiran, R. Meuli, and M. B. Cuadra, "An efficient total variation algorithm for super-resolution in fetal brain MRI with adaptive regularization," *NeuroImage*, vol. 118, pp. 584–597, Sep. 2015.
[24] J. Wright, A. Y. Yang, A. Ganesh, S. S. Sastry, and Y. Ma, "Robust face recognition via sparse representation," *IEEE Trans. Pattern Anal. Mach. Intell.*, vol. 31, no. 2, pp. 210–227, Feb. 2009.
[25] J. Yang, J. Wright, T. S. Huang, and Y. Ma, "Image super-resolution via sparse representation," *IEEE Trans. Image Process.*, vol. 19, no. 11, pp. 2861–2873, Nov. 2010.
[26] I. Bayram and I. W. Selesnick, "A subband adaptive iterative shrinkage/thresholding algorithm," *IEEE Trans. Signal Process.*, vol. 58, no. 3, pp. 1131–1143, Mar. 2009.
[27] Q. Zhang, Y. Zhang, D. Mao, Y. Zhang, Y. Huang, and J. Yang, "A Bayesian super-resolution method for forward-looking scanning radar imaging based on split bregman," in *Proc. IEEE Int. Geosci. Remote Sens. Symp. (IGARSS)*, Jul. 2018, pp. 5135–5138.
[28] Y. Zha, Y. Huang, and J. Yang, "Augmented Lagrangian method for angular super-resolution imaging in forward-looking scanning radar," *J. Appl. Remote Sens.*, vol. 9, no. 1, 2015, Art. no. 096055.
[29] D. R. Hunter and K. Lange, "A tutorial on MM algorithms," *Amer. Statist.*, vol. 58, no. 1, pp. 30–37, 2004.
[30] M. A. T. Figueiredo, J. M. Bioucas-Dias, and R. D. Nowak, "Majorization–minimization algorithms for wavelet-based image restoration," *IEEE Trans. Image Process.*, vol. 16, no. 12, pp. 2980–2991, Dec. 2007.
[31] M. K. P. Ng, R. H. Chan, and W.-C. Tang, "A fast algorithm for deblurring models with Neumann boundary conditions," *SIAM J. Sci. Comput.*, vol. 21, no. 3, pp. 851–866, 1999.
[32] R. W. Freund and H. Zha, "A look-ahead algorithm for the solution of general Hankel systems," *Numerische Mathematik*, vol. 64, no. 1, pp. 295–321, 1993.
[33] D. S. C. Biggs and M. Andrews, "Acceleration of iterative image restoration algorithms," *Appl. Opt.*, vol. 36, no. 8, pp. 1766–1775, 1997.
[34] A. Beck and M. Teboulle, "A fast iterative shrinkage-thresholding algorithm for linear inverse problems," *SIAM J. Imag. Sci.*, vol. 2, no. 1, pp. 183–202, 2009.
[35] Q. Zhang, Y. Zhang, Y. Huang, and Y. Zhang, "Azimuth superresolution of forward-looking radar imaging which relies on linearized bregman," *IEEE J. Sel. Topics Appl. Earth Observ. Remote Sens.*, to be published. doi: 10.1109/JSTARS.2019.2912993.
[36] Z. Lin, M. Chen, and Y. Ma, "The augmented Lagrange multiplier method for exact recovery of corrupted low-rank matrices," Sep. 2010, *arXiv:1009.5055*. [Online]. Available: https://arxiv.org/abs/1009.5055
[37] I. Selesnick, "Total variation denoising (an MM algorithm)," in *NYU Polytechnic School of Engineering Lecture Notes*. New York, NY, USA: New York Univ., 2012.
[38] Y. Zha, Y. Huang, Z. Sun, Y. Wang, and J. Yang, "Bayesian deconvolution for angular super-resolution in forward-looking scanning radar," *Sensors*, vol. 15, no. 3, pp. 6924–6946, Jan. 2015.
[39] P. C. Hansen and D. P. O'Leary, "The use of the L-curve in the regularization of discrete ill-posed problems," *SIAM J. Sci. Comput.*, vol. 14, no. 6, pp. 1487–1503, Apr. 1993.
[40] T. Long, Z. Lu, Z. Ding, and L. Liu, "A DBS Doppler centroid estimation algorithm based on entropy minimization," *IEEE Trans. Geosci. Remote Sens.*, vol. 49, no. 10, pp. 3703–3712, Oct. 2011.
[41] D. Donoho, "On minimum entropy deconvolution," in *Applied Time Series Analysis II*. Amsterdam, The Netherlands: Elsevier, 1981, pp. 565–608.

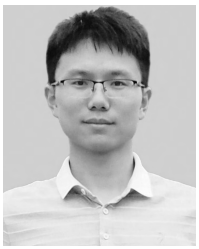

QIPING ZHANG (S'17) received the B.S. degree in electronic information engineering from Yunnan University, Kunming, China, in 2016. He is currently pursuing the Ph.D. degree with the University of Electronic Science and Technology of China, Chengdu, China. His research interests include signal processing and radar imaging.

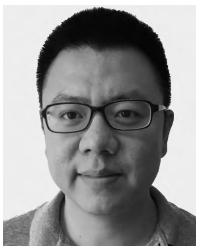

YIN ZHANG (S'13–M'16) received the B.S. and Ph.D. degrees in electronic information engineering from the University of Electronic Science and Technology of China (UESTC), Chengdu, China, in 2008 and 2016, respectively.

From 2015 to 2016, he was a Visiting Student with the University of Delaware, Newark, DE, USA. He is currently an Associate Research Fellow with the School of Information and Communication Engineering, UESTC. His research interests include radar imaging and signal processing in related radar applications.

YULIN HUANG (M'08–SM'17) received the B.S. and Ph.D. degrees from the School of Electronic Engineering, University of Electronic Science and Technology of China (UESTC), Chengdu, China, in 2002 and 2008, respectively.

From 2013 to 2014, he was a Visiting Researcher with the University of Houston, Houston, TX, USA. He is currently a Professor with the School of Information and Communication Engineering, UESTC. His research interests include synthetic aperture radar, target detection and recognition, artificial intelligence, and machine learning.

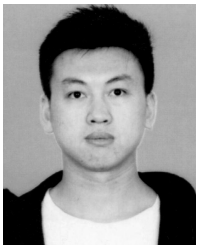

YONGCHAO ZHANG (S'15–M'18) received the B.S. degree in electronic information engineering from Hainan University, Haikou, China, in 2011, and the Ph.D. degree from the School of Information and Communication Engineering, University of Electronic Science and Technology of China (UESTC), Chengdu, China, in 2018.

From 2016 to 2017, he was a Visiting Student with Lund University, Lund, Sweden. He is currently an Associate Research Fellow with the School of Information and Communication Engineering, UESTC. His research interests include array signal processing and inverse problem in radar applications.

WENCHAO LI (M'13) received the Ph.D. degree in electronic engineering from the University of Electronic Science and Technology of China (UESTC), Chengdu, China, in 2012.

He is currently an Associate Research Fellow with the School of Information and Communication Engineering, UESTC. He is also a Visiting Researcher with The Ohio State University, Columbus, OH, USA. His research interests include radar imaging and motion compensation.

JIANYU YANG (M'06) received the B.S. degree from the National University of Defense Technology, Changsha, China, in 1984, and the M.S. and Ph.D. degrees from the University of Electronic Science and Technology of China (UESTC), Chengdu, China, in 1987 and 1991, respectively.

He is currently a Professor with UESTC. His research interests include synthetic aperture radar and statistical signal processing. He serves as a Senior Editor for the *Chinese Journal of Radio Science* and the *Journal of Systems Engineering and Electronics*.